JOURNAL OF CATALYSIS **164,** 220–231 (1996)
ARTICLE NO. 0377

# Catalytic Properties of Oxygen Semipermeable Perovskite-Type Ceramic Membrane Materials for Oxidative Coupling of Methane

Y. S. Lin[1] and Y. Zeng

*Department of Chemical Engineering, University of Cincinnati, Cincinnati, Ohio 45221-0171*

Received March 15, 1996; revised July 31, 1996; accepted August 1, 1996

**The catalytic properties for the oxidative coupling of methane (OCM) of $La_{0.8}Sr_{0.2}CoO_3$ (LSC) and $SrCo_{0.8}Fe_{0.2}O_3$ (SCF) in solid solution were studied and compared with those of 5 wt% Li/MgO, using a steady/unsteady state packed-bed reactor and a transient microbalance. The results of the steady-state cofeed experiments show that LSC possesses OCM catalytic properties similar to those of Li/MgO in terms of $C_2$ yield and selectivity at temperatures of around 800°C. The former gives a larger $C_2$ space time yield than the latter. SCF exhibits poor OCM catalytic properties at 700–850°C. To further examine the suitability of LSC as a membrane material for use in a dense membrane reactor for OCM, the instant OCM selectivity and activity and oxygen consumption rate for LSC and 5% Li/MgO on exposure to pure methane in cyclic feed mode were measured respectively at 850°C and 800°C. For both materials, the unsteady-state cyclic feed operation gives smaller initial OCM activity and larger initial $C_2$ selectivity than the cofeed steady state operation. Li/MgO quickly loses its OCM activity and selectivity in the unsteady state operation due to rapid consumption of the active sites. Up to 5 min of methane run time, LSC maintains appreciable OCM activity with poorer $C_2$ selectivity as compared to the steady state cofeed operation. The surface of LSC membrane at low oxygen partial pressure may become nonselective for OCM in membrane reactor applications.** 

## INTRODUCTION

Significant efforts have been reported in the past decade toward the development of new catalysts for oxidative coupling of methane (OCM). However, the intrinsic limit on the $C_2$ yield in a fixed-bed reactor is around 25% (1). Some alternate reactor configurations have been proposed and studied recently in order to improve the $C_2$ yield. These include the work of Carr and co-workers on a simulated countercurrent moving-bed chromatographic reactor (2, 3), and that of Vayenas and co-workers on a gas recycle electrocatalytic reactor (4). Very high overall $C_2$ yields (>60%) were achieved for OCM in these reactors. But the conversion of $CH_4$ per pass in the reactors was actually controlled to be very low. The use of separation units in the reactors and the recycling of a large amount of reactants and products make the processes more complicated and economically less attractive.

Membrane reactors have attracted increasing attention in the scientific community for OCM because they offer several advantages for partial oxidative reactions, i.e., simplicity in process design, safety in operation, and, most importantly, the possibility of achieving higher $C_2$ selectivity as well as yield. In recent years, a few studies have been reported attempting to improve the $C_2$ selectivity for OCM at higher methane conversion by using ceramic membrane reactors (5–17). The studies in this area can be divided into two groups: those using dense ionic-conducting membrane reactors and those using porous ceramic membrane reactors. For OCM in the dense ionic-conducting membrane reactor, methane is brought into contact with one surface of the dense membrane and reacts with the oxygen permeating from the other surface. Results of OCM in membrane reactors made of 10% $Y_2O_3$–89% $ZrO_2$–1% $TiO_2$ (5, 6), yttria stabilized zirconia (8, 10), $CaCo_{0.8}Fe_{0.2}O_3$ (9), $La_{0.6}Sr_{0.4}Co_{0.8}Fe_{0.2}O_3$ (14), and yttria stabilized zirconia with an external electric circuit (solid oxide fuel cell structure) (15–17) have been reported in the patent and open literature. In general, the dense membrane reactors give a higher $C_2$ selectivity (60–90%), but with a lower $C_2$ yield per pass (0.5%–30%). In the second group, Santamaria and co-workers (11, 12) studied OCM in a porous alumina membrane reactor packed with an OCM catalyst (e.g., Li/MgO). The basic idea was to use the membrane to control the $O_2/CH_4$ ratio at the optimum value along the axial direction of the reactor in order to increase the overall hydrocarbon selectivity without decreasing the $CH_4$ conversion. The experimental results showed a higher $C_2$ selectivity as compared with the conventional reactor. However, the improvement on the $C_2$ yield is not significant. A similar concept was also recently applied to oxidative dehydrogenation of ethane using porous ceramic membranes (18) and partial oxidative reaction of methane for syngas synthesis using dense mixed-conducting ceramic membranes (19, 20).

In the porous membrane reactor for OCM, the membrane serves as an oxygen distributor, and methane reacts

[1] To whom correspondence should be addressed.



0021-9517/96 $18.00

with oxygen in a manner identical to that in the conventional packed-bed reactor. As a result, the performance of OCM in the porous membrane reactor strongly depends on the kinetics of OCM on the catalyst used and the distribution of oxygen permeance along the axial direction. The principle of OCM in a dense membrane reactor is fundamentally different from that in the porous membrane reactor. In the dense membrane reactor, methane is adsorbed and activated on the membrane surface, and the resulting intermediate carbon containing species are coupled to form $C_2$, occurring most likely in the gas phase. The catalytic properties of the membrane surface, oxygen permeance of the membrane, and operating conditions are critical to the performance of the dense membrane reactor for OCM. These, however, were not properly addressed in the previous work.

In order to achieve significantly improved $C_2$ yield for OCM in the dense membrane reactor, Wang and Lin (21) recently proposed the use of an ionic-conducting dense membrane with a surface which is catalytically active and selective for OCM in a dense membrane reactor. With such a membrane, the oxygen permeating from the other side of the membrane may directly replace the oxygen in the active sites consumed in the methane activation process. If the oxygen permeance through the membrane is controlled to be comparable to the consumption rate of oxygen in the reactor, complete oxidation reactions on the membrane surface as well as in the gas phase can be minimized, resulting in an extremely high $C_2$ selectivity for OCM in the membrane reactor (21). For a given membrane material, the oxygen permeance can be controlled by selection of proper operating conditions or synthesis of membranes with different thicknesses (only possible above the critical value when the surface reaction is not the rate limiting step) (22). Thus, the selection of a membrane material with good intrinsic OCM catalytic properties becomes the most critical step in the development of dense membrane reactors for OCM.

In the previously studied dense membrane reactors, dense membrane (or electrolyte) materials *per se* do not possess proper catalytic properties for OCM (5, 6, 8–10). The particles of OCM catalysts (e.g., Li/MgO) were coated on the membrane (or electrolyte) surface exposed to the methane stream in order to introduce specific OCM catalytic properties. Because of the existence of the complicated interfacial structure between the coated catalyst particles and membrane surface (three phase boundary), such membrane composites do not resemble the oxygen-semipermeable membrane layer the surface of which is catalytically active and selective for OCM. In the case of OCM catalyst coated membrane, oxygen having permeated through the membrane may get into the gas phase before being adsorbed onto the surface of the coated catalytic particles, resulting in further oxidation of methyl radicals or $C_2$ products in the gas phase. So it was difficult to achieve a higher $C_2$ yield in this type of dense membrane reactor.

Although many different types of catalysts have been found to posses good catalytic properties for OCM, most of them do not qualify as membrane materials. Three better known groups of oxygen semipermeable ionic-conducting ceramic materials are the zirconia based, bismuth oxide based, and perovskite-type ceramics (23). Among the various perovskite-type oxides, $La_{1-y}Sr_yCo_{1-x}Fe_xO_3$, especially $La_{0.8}Sr_{0.2}CoO_3$ and $SrCo_{0.8}Fe_{0.2}O_3$, were most extensively studied for their oxygen permeation properties (24–27). The permeability data reported by the different investigators, though somewhat inconsistent, show that $SrCo_{0.8}Fe_{0.2}O_3$ membrane is most oxygen semipermeable among the various ceramic membranes reported so far. Some data on the OCM catalytic properties of $La_{1-y}Sr_yCoO_3$ and $SrCo_{0.8}Fe_{0.2}O_3$ were also published recently (29, 30). But the data reported are too limited and, in some cases, inconsistent among the different investigators. For example, Alcock *et al.* (29) found that for OCM reaction at about 800°C the perovskite-type oxides with high *p*-type electronic conductivity (including $La_{0.8}Sr_{0.2}CoO_3$) did not yield any $C_2$ products, but Ten Elshof *et al.* (14) reported considerable activity and selectivity for OCM on $La_{0.6}Sr_{0.4}Fe_{0.2}O_3$. The exact OCM catalytic properties of these membrane materials are not clear.

In the present work, OCM catalytic properties of two oxygen semipermeable membrane materials $La_{0.8}Sr_{0.2}CoO_3$ and $SrCo_{0.8}Fe_{0.2}O_3$ were systematically investigated in order to evaluate their suitability as the membrane materials for the OCM membrane reactors. One of the best studied OCM catalysts, Li/MgO, was also examined in this work for comparison.

## EXPERIMENTAL

$La_{0.8}Sr_{0.2}CoO_3$ and $SrCo_{0.8}Fe_{0.2}O_3$ powders were synthesized by a liquid citrate method (25, 31). These powders were prepared by dissolving the stoichiometric amounts of appropriate metal nitrates in a dilute nitric acid solution, followed by adding citric acid with the pH adjusted to the range of 3–5 by addition of $NH_4OH$. The resulting solution was then evaporated on a hot plate until pyrolysis took place. The powders were calcined at 1000–1100°C. A 5 wt% Li doped MgO powder was prepared by a wet impregnation method reported in the literature (32, 33). In preparing the catalyst, MgO (99%, Aldrich) and $LiCO_3$ (99%, Aldrich) were added to deionized water, which was evaporated while stirring at room temperature until only a thick paste remained. The paste was dried overnight in air at 140°C and then calcined in air at 850°C for 6 h. After calcination, the oxides were crushed into small particles (0.1–0.3 mm). The BET surface areas of the oxide samples were determined by the nitrogen adsorption

method (Micromeritics ASAP 2000). The phase structures of the catalysts were examined by the X-ray diffraction (Siemens Kristalloflex D500 diffractometer, with Cu$K\alpha$ radiation).

The OCM catalytic properties of the catalysts were studied in a packed-bed reactor made of a dense alumina (99.8%) tube (ID = 1/4 in., length = 22 in.). Methane (99.9%), oxygen (99.9%), and helium (99.9%) (all from Matheson Gas Inc.) were used as the feed gases. The catalyst was packed in the middle portion of the alumina tube and supported by quartz particles (0.5 mm diameter) from the two sides. The compositions of the feed and product gases where analyzed by gas chromatography using a Carbosphere column (10 ft long, 1/8 in. in diameter, with 80/100 mesh packing materials).

In the cofeed experiments, a gas stream containing methane, oxygen, and helium at a given composition and flow rate was fed into the reactor. Effluent composition was measured after the system reached the steady state. In the cyclic mode experiments, oxygen, helium, and methane were sequentially fed into the reactor. Before methane was introduced, helium was passed through the reactor to purge oxygen out of the gas phase. The oxygen and helium run times were respectively 5 min and 30 s. At time zero, methane at a constant flow rate was introduced into the reactor by switching the feed stream from helium to pure methane. Under the reaction conditions, typical residence time for methane in the reactor tube was less than 2 s. The effluent from the reactor was intermittently sampled by a 10 ports rotary valve (Valco Instruments), and analyzed by gas chromatography. Due to the possible effects on the flow pattern of switching the gas stream from helium to methane, the composition data of the effluent samples obtained within the first 10 s of the methane run may not be very accurate, and therefore are not included in the results presented next.

The methane conversion is defined as the percentage of methane converted to products and calculated by

$$C = (Q_{\text{in}}X_{\text{CH}_4} - Q_{\text{out}}Y_{\text{CH}_4})/Q_{\text{in}}X_{\text{CH}_4}, \qquad [1]$$

where $Q$ stands for the volumetric flow rate and $X$ and $Y$ are molar fractions in the feed and effluent, respectively. The selectivity for the carbon containing product $i$ is the percentage of reacted methane that forms product $i$ and is calculated by

$$S_i = (Q_{\text{out}}n_iY_i)/(Q_{\text{in}}X_{\text{CH}_4} - Q_{\text{out}}Y_{\text{CH}_4}), \qquad [2]$$

where $n_i$ is the number of carbon atoms in the molecule of the carbon containing product $i$. The $C_2$ yield is the percentage of total methane that forms ethane and ethylene, which can be calculated from the product of methane conversion and $C_2$ selectivity. In the cyclic feed experiments, the instant formation rates for product $i$ at the time of sampling were calculated from the total molar flow rate and molar fraction of the species of the effluent, $M_{\text{out}}$, and $Y_i$ by

$$R_i = M_{\text{out}}Y_i/W_{\text{cat}} \qquad [3]$$

where $W_{\text{cat}}$ is the weight of catalyst.

In the cofeed experiments, the difference of carbon mass balance between the inlet and outlet was found to be less than 5%. In the temperature range investigated the results of the cofeed experiments in the alumina tube packed with quartz without catalyst show less than 2% yield for ethane and carbon oxides and no ethylene in the effluent. This indicates that quartz packed in the alumina tube is catalytically inert to OCM, and the noncatalytic reactions in the empty space of the quartz-packed reactor tube contribute negligibly to the OCM results. The methane conversion in the cyclic feed mode under the studied experimental conditions was less than 5%.

The transient TGA experiments were carried out in a high temperature microelectronic recording balance system (Cahn 1000), as shown in Fig. 1. A quartz sample pan was hanged inside a 2 in.d. quartz reactor tube of which the sample zone could be heated up to 1000°C by a furnace surrounding the tube. The temperature was measured by a thermocouple placed on the outer surface of the reactor tube. The sample weight, reactor temperature, and pressure were recorded by a PC using data acquisition software (Strawberry). In the experiments, a given amount of catalyst powder (about 450 mg for Li/MgO and 350 mg for LSC) was put in the sample pan. The sample was heated from the room temperature to the desired temperature under a flow of pure $O_2$ at 1 atm. After the sample weight reached the steady state value at the desired temperature, the surrounding stream was changed to another gas. The corresponding transient sample weight changes were recorded. The flow rate of the gas fed from the bottom of the quartz tube was 200 ml (STP)/min for $O_2$ and He, and 50 ml (STP)/min for $CH_4$. Extreme care was taken to ensure that the system was leakage-free during experiments to avoid direct contact of methane with air at high temperatures. Otherwise possible explosion could occur.

## RESULTS AND DISCUSSION

### *Steady-State Study*

The XRD patterns of $La_{0.8}Sr_{0.2}CoO_3$ (LSC), $SrCo_{0.8}\cdot Fe_{0.2}O_3$ (SCF), and Li/MgO are shown in Fig. 2. The XRD of Li/MgO reflects a major cubic MgO phase with trace amount of $Li_2O$ phase, indicating that solid solution was not formed in this sample. Both SCF and LSC have the desired cubic perovskite phase structure. The preparation method and XRD data show that the SCF and LSC samples are in the form of solid solution and the Li/MgO sample consists of a lithium oxide layer coated on the surface of MgO

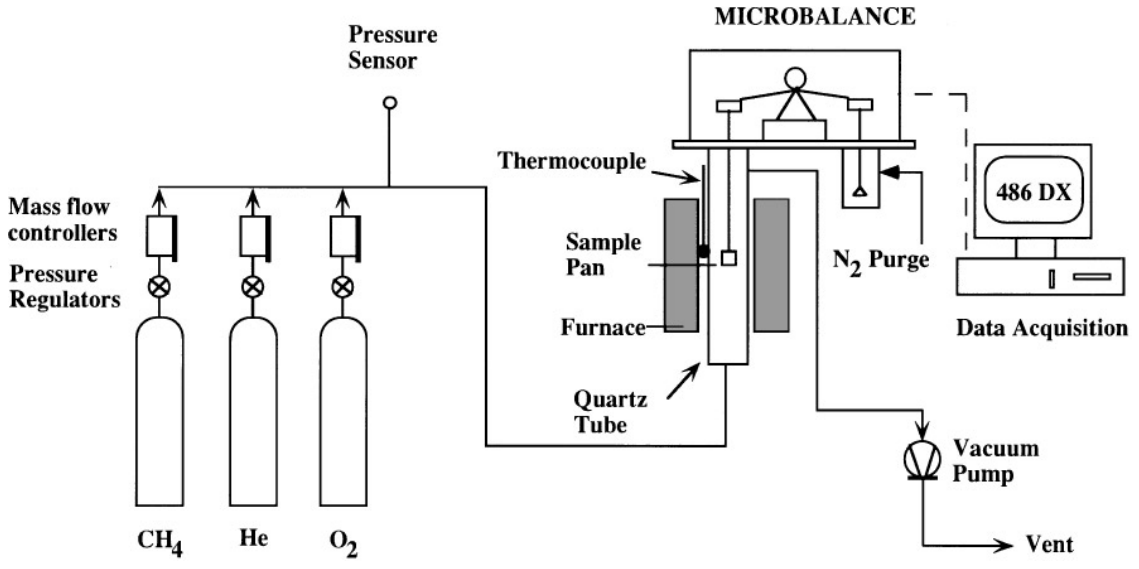


**FIG. 1.** Schematic diagram of electronic microbalance system for transient TGA study.

particles. Table 1 summarizes the characteristics of the three catalysts studied in this work.

It is known that operating conditions, such as reaction temperature, methane to oxygen ratio and feed flow rate, have strong effects on the results of OCM on a catalyst. In this study it was found that the $C_2$ selectivity decreased slightly and the methane conversion increased significantly with decreasing methane to oxygen ratio when it is larger than 3. The ratio of the stoichiometric coefficient of methane to that of oxygen in the ethylene formation reaction is 2. In this work a methane to oxygen ratio of 2.9 was selected for the cofeed experiments. The $C_2$ yields at this methane/oxygen ratio were measured for the three catalysts at different flow rates and temperatures. The optimum flow rate and temperature corresponding to the maximum $C_2$ yield were found for each catalyst. These optimum conditions for the three catalysts are listed in Table 1. As shown in the table, the optimum temperatures and flow rates are different among the three catalysts because of their different catalytic properties. Since the main objective of this work is to identify a perovskite-type membrane material with desired OCM properties for membrane reactor application, all cofeed experiments reported in this study were conducted under the conditions listed in Table 1.

**TABLE 1**

**Characteristics and OCM Properties of Solid Oxide Materials Studied in This Work ($CH_4 : O_2 : He = 2.9 : 1 : 1.3$)**

| Material formula | $La_{0.2}Sr_{0.8}CoO_{3-\delta}$ | $SrCo_{0.8}Fe_{0.2}O_{3-\delta}$ | 5 wt% Li/MgO |
|---|---|---|---|
| Abbreviation | LSC | SCF | Li/MgO |
| Structure | Perovskite solid solution | Perovskite solid solution | $Li_2O$ coated MgO crystals |
| Surface area ($m^2$/g) | 0.9 | 0.3 | 5.1 |
| Amount packed in reactor (g) | 0.40 | 0.10 | 0.30 |
| Flow rate[a] (ml(STP)/min) | 99 | 48 | 8 |
| Reaction temp[a] (°C) | 800 | 850 | 800 |
| Maximum $C_2$ yield (%) | 14.0 | 6.3 | 19.3 |
| $C_2$ space time yield ($\mu$mol/g · s) | 7.2 | 6.3 | 1.1 |
| $C_2$ selectivity (%) | 40 | 30.4 | 51.4 |

[a] Optimal value maximizing $C_2$ yield.

Figures 3 and 4 show the $C_2$ yield and selectivity as a function of temperature. These cofeed steady-state experimental results show that Li/MgO has the highest $C_2$ yield (19.3%) and selectivity (57%) among the three catalysts. In the 700–800°C temperature range, the $C_2$ selectivity for Li/MgO slightly decreases, while $C_2$ yield increases with increasing temperature. This result is consistent with other reports (27, 33). In the range 700–830°C, LSC also exhibits fairly good catalytic properties. At 830°C the $C_2$ selectivity for LSC is 54%. The highest $C_2$ yield for LSC is 14% at 800°C. It should be noted that the activity of the LSC decreases as temperature increases from 800°C to 830°C. This is not consistent with the general rule for OCM (34–37). This might be caused by a surface property change of LSC in this temperature range in which the activity of the LSC for $CO_x$ formation dramatically decreases. SCF exhibits, however, very poor $C_2$ yield and selectivity for OCM. At high temperatures the $C_2$ yield and selectivity for OCM on SCF are similar to those for OCM in an empty reactor tube.

A comparison of the percentage of $C_2H_4$ over the total $C_2$ products for the three catalysts in different temperatures is given in Fig. 5. It shows that $C_2H_4$ percentage

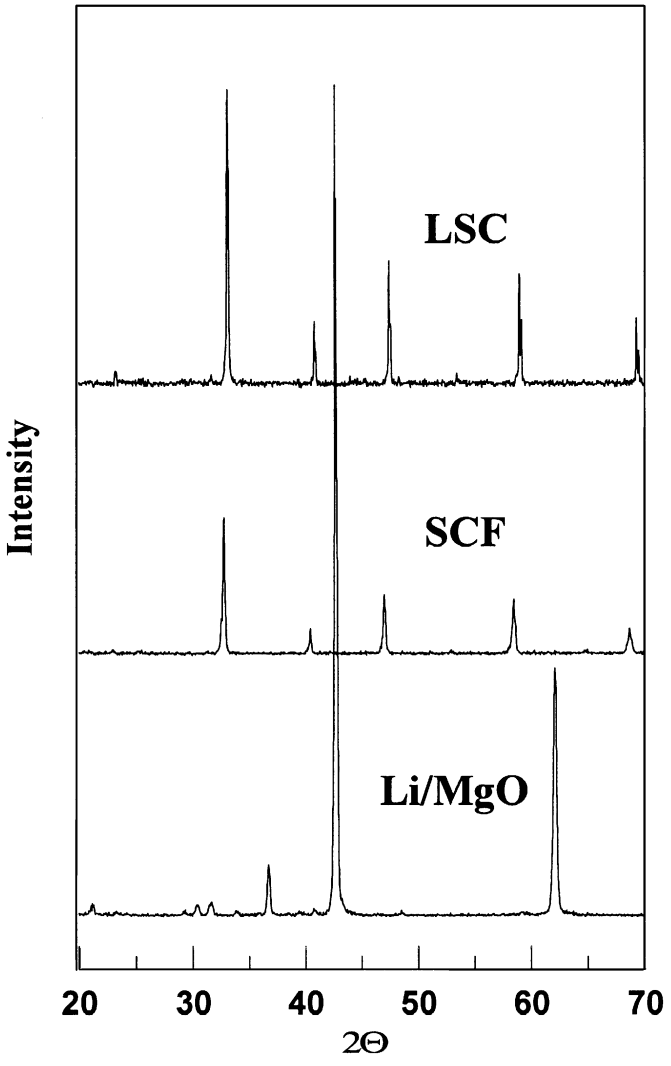


**FIG. 2.** XRD patterns of three solid oxide materials studied in this work.

generally increases with increasing temperature. Li/MgO exhibits the highest $C_2H_4$ percentage (80%) at 800°C. The $C_2H_4/C_2H_6$ ratio for LSC and SCF is lower as compared with Li/MgO. Nevertheless SCF and LSC still give more ethylene (roughly about 60%) in the $C_2$ products (at 830°C). The percentage of CO in $CO_x$ for the three materials are given in Fig. 6. This percentage decreases in the order Li/MgO > SCF > LSC. All three catalysts give more $CO_2$ than CO, indicating that undesired reactions lead mostly to complete oxidation of methane.

The activity of the OCM catalysts is better represented by the $C_2$ space time yield (or $C_2$ formation rate) defined as the molar formation rate of the $C_2$ products per unit weight of catalyst (1, 34). The results of the $C_2$ space time yield for the three catalysts at the flow rates listed in Table 1 are shown in Fig. 7. It is interesting to note that in this case Li/MgO has the smallest $C_2$ space time yield (1.1 $\mu$mol/g · s) at 800°C. With a much smaller surface area than Li/MgO, the two

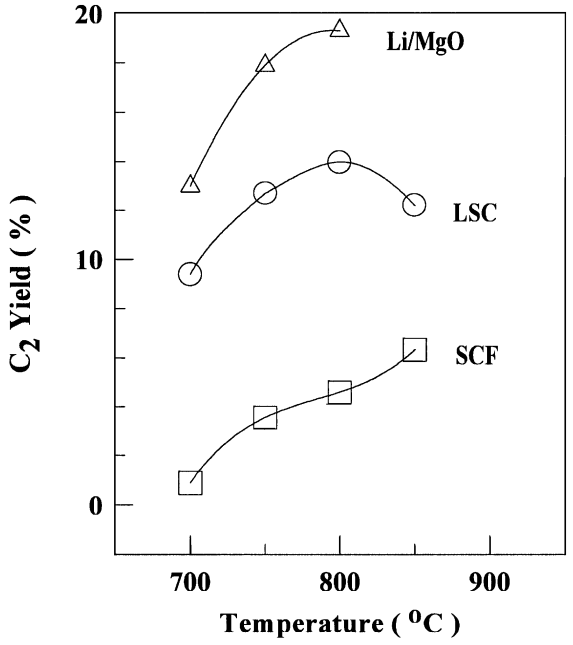


**FIG. 3.** Comparison of cofeed $C_2$ yield on three oxide materials.

perovskite type ceramics, especially LSC, exhibit very high $C_2$ space time yield. This indicates the high catalytic activity of the perovskite-type ceramics.

It is generally agreed that the catalytically oxidative coupling of methane undergoes the dissociation of methane into methyl radical at the active sites on the catalyst surface. These active sites are usually reactive oxygen species (e.g., $O^-$, $O_2^{2-}$) and lattice oxygen species ($O^{2-}$). For alkali

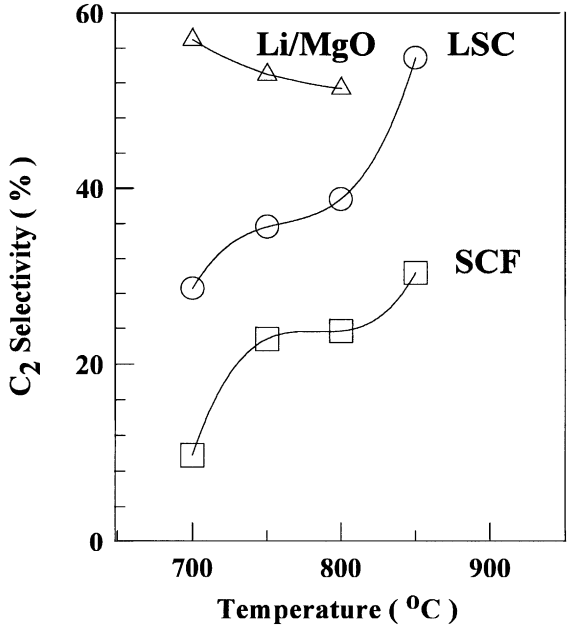


**FIG. 4.** Comparison of cofeed $C_2$ selectivity on three oxide materials.

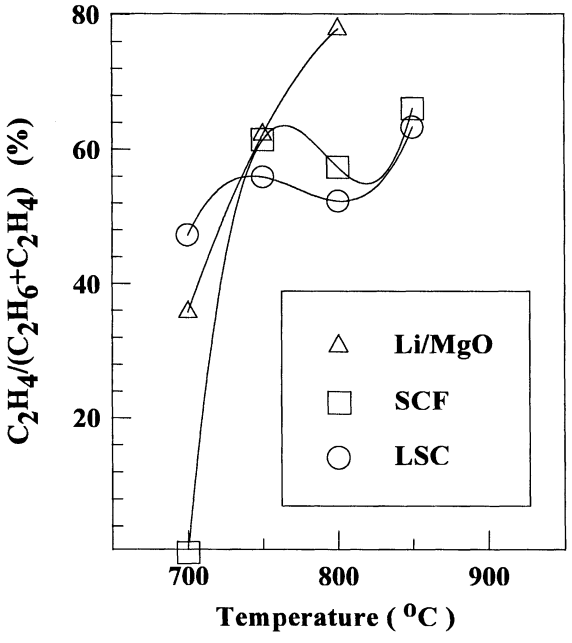


**FIG. 5.** Comparison of percentage of $C_2H_4$ in total $C_2$ products for three oxide materials obtained in the cofeed experiments.

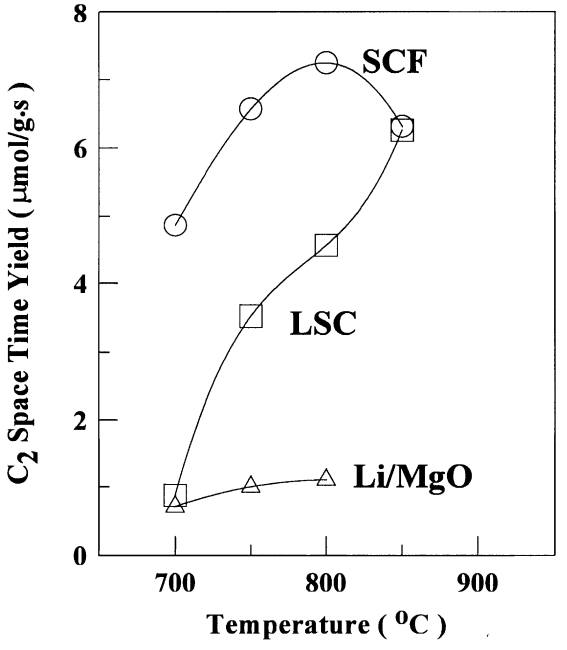


**FIG. 7.** $C_2$ space time yield ($C_2$ formation rate) for OCM on the three metal oxides.

promoted alkaline earth oxide catalysts, like Li/MgO, the reactive oxygen species such as $O^-$ or $O^{2-}$ ions on the surface are effective in abstracting hydrogen atom from the methane molecule to form $CH_3$ radicals (32). These radicals then release into the gas phase in which they are coupled to form $C_2$ hydrocarbons.

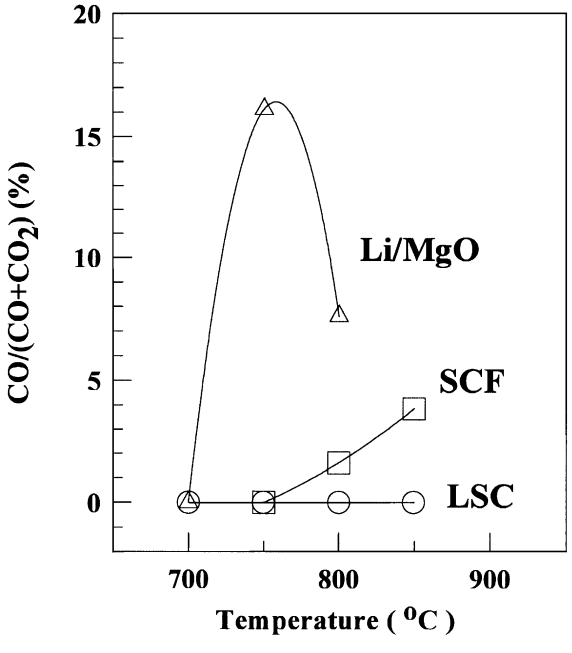


**FIG. 6.** Comparison of percentage of CO in total $C_1$ products for three oxide materials obtained in the cofeed experiments.

The partial oxidation of methane on perovskite-type oxides is not well understood. Baerns and co-workers (38) pointed out that *p*-type electronic-conducting materials generally have better $C_2$ selectivity than *n*-type ones. The oxygen partial pressure from the inlet to the outlet of the reactor in the cofeed study, estimated from the $CH_4/O_2$ ratio in the feed stream and the $CO/CO_2$ ratio in the effluent, ranged from $10^{-1}$ to $10^{-17}$ atm. In this range of oxygen partial pressure, LSC primarily remains a *p*-type electronic conductor while SCF may have changed to an *n*-type one (39). The present experimental results for LSC and SCF are consistent with those found by Baern and co-workers on *p*-type and *n*-type electronic conductors. However, Alcock *et al.* (29) found that for OCM reaction at about 800°C the small surface area perovskite-type oxides with high *p*-type electronic conductivity (including $La_{0.8}Sr_{0.2}CoO_3$) did not yield any $C_2$ products, while those with *n*-type electronic conductivity exhibited significant activity for OCM reaction with low $C_2$ selectivity. This was probably because a feed containing 30% $CH_4$ + 5% $O_2$ + 65% He was used in their study. This could result in an extremely low oxygen partial pressure in the gas phase ($<10^{-19}$ atm) under which the *p*-type ceramic electronic conductors may become *n*-type ones or decompose.

McCarty and Wise (37) prepared $La_{0.5}Sr_{0.5}CoO_3$ with a relatively large surface area (7–100 $m^2/g$) and showed that the perovskite type oxide was a good catalyst for complete oxidation of methane at temperatures higher than 800°C. This result is different from the present study, due probably to the fact that the surface area of their catalyst is much

larger than that of the LSC samples used in the present work. The perovskite-type material used in the above study was prepared by the conventional solid-state method, with which it is difficult to obtain a dense ceramic in solid solution form, as compared with the citrate method. Hayakawa *et al.* (28) reported a $C_2$ selectivity of about 30% for OCM on $La_{0.6}Sr_{0.4}CoO_3$ at 700°C. This is similar to the present result for $La_{0.8}Sr_{0.2}CoO_3$ at 700°C. The perovskite-type oxides used in the study of Hayakawa *et al.* were prepared by the same citrate method as employed in the present work. These results show that similar perovskite materials prepared by different methods exhibit very different catalytic properties for OCM.

It is suggested that the absorbed oxygen (oxygen filled in the oxygen vacancies of the oxide) is much more reactive for formation of $C_2$ than the lattice oxygen (37–40), due to the high mobility of the nonstoichiometric oxygen. Some electrochemical properties for the two perovskite-type catalysts studied are summarized in Table 2. The transport rate of the nonstoichiometric oxygen (equivalent to permeability) of the perovskite-type oxide is roughly proportionally to bulk conductivities $[\sigma_i\sigma_e/(\sigma_i+\sigma_e)]$ and oxygen surface exchange rate, as detailed in Refs. (22, 48). For the small perovskite-type ceramic particles used in this study, the resistance of bulk diffusion is smaller than that of surface reaction. Thus, the transport rate of the nonstoichiometric oxygen is more likely limited by the oxygen surface exchange rate, which increases with increasing temperature. The fact that LSC has better OCM properties than SCF in consistent with the larger oxygen surface exchange rate of LSC than SCF, as shown in Table 2.

The present study and the previous work (25, 34–37) appear to support the following general rules for OCM on the perovskite-type ceramic oxides: (1) a high transport rate of oxygen in the bulk ceramic and on the ceramic surface favors OCM reaction activity; (2) *p*-type electronic conduction mechanisms give better selectivity for OCM than *n*-type mechanisms; (3) high surface area of catalysts leads to complete oxidation reactions; (4) preparation methods also affect the OCM properties of perovskite-type oxides.

Good OCM catalytic properties of LSC observed in the fixed-bed reactor operated in the steady state cofeed mode do not necessarily mean that it will have the same catalytic properties when operated under membrane reactor conditions. With respect to carbon oxide formation reactions, the steady-state cofeed experiments cannot distinguish the surface reaction from the gas phase reaction. Since synthesis of membranes and experiments on membrane reactor are difficult, it is certainly more desirable to develop a method that avoids the membrane synthesis and membrane reactor experiments for evaluating the catalytic properties of membrane materials. The OCM properties of the membrane material obtained in the cyclic feed mode are closer to those of the membrane made of the same material when operated in the membrane reactor. The following section is focused on the unsteady-state study of OCM on LSC only since it exhibits much better OCM catalytic properties than SCF. Li/MgO was also studied for comparison.

**TABLE 2**

**Electrochemical Properties of the Perovskite Type Ceramics Studied in This Work (at 800°C)**

| Properties | LSC | SCF | Ref. |
|---|---|---|---|
| Ionic conductivity (in air) $\sigma_i$ (S/cm) | 0.31 | 1.3 | (23) |
| Electronic conductivity (in air) $\sigma_e$ (S/cm) | 690 | 130 | (23) |
| $O_2$ surface exchange rate (mol/m$^2\cdot$s) | $6.4\times10^{-3}$ | $1.2\times10^{-3}$ | (48) |

*Unsteady-State Study*

The cyclic feed operation was first employed in the pioneering work of Keller and Bhasin (41), and subsequently by several others to explore the feasibility of achieving higher $C_2$ yield by unsteady state operation (e.g, 43) or to study OCM reaction mechanisms (e.g., 44). In the cyclic feed mode, oxygen, purge gas, and methane are sequentially fed into a reactor packed with the metal oxide catalyst. The metal oxide particles retain the oxygen from the oxygen stream and react with methane to form $C_2$ products and $CO_x$ when methane is introduced. Purge gas is used between the oxygen and methane runs in order to sweep the gas phase oxygen from the reactor bed. The cyclic feed mode minimizes the presence of oxygen in the gas phase when methane is brought into contact with the metal oxide particles. This would substantially reduce the carbon oxide formation reaction in the gas phase. The similarities between the OCM reaction in a packed-bed reactor operated in the cyclic feed mode and that in a membrane reactor include the following: (1) feed streams are separated; (2) carbon oxide formation reactions in the gas phase are minimized; (3) catalyst activity is regenerated during the operation and (4) catalyst is exposed to highly reducing environment. The major differences between the membrane reactor and the packed-bed reactor operated in the cyclic mode are (1) the former is a steady-state process while the latter is an unsteady-state one; (2) the catalyst in the latter undergoes periodical reduction and oxidation reactions while the membrane in the former does not experience these changes.

The cyclic operation conditions for LSC and Li/MgO are summarized in Table 3. The reaction temperatures selected correspond to the highest $C_2$ yield observed in the cofeed study. During the methane run, the effluent gas from the reactor packed with either LSC or Li/MgO contained primarily ethylene, ethane, methane, carbon dioxide, and water vapor. There was essentially no carbon monoxide in the effluent stream. The instant formation rates of $C_2$ products and carbon oxides on LSC and Li/MgO as a function of the methane run time are shown in Fig. 8. The corresponding

**TABLE 3**

**Summary of the Results of OCM in Cyclic Mode in the First 4-min Methane Run**

| | $La_{0.2}Sr_{0.8}CoO_3$ | 5% Li/MgO |
|---|---|---|
| Catalyst amount (g) | 0.40 | 0.60 |
| Surface area ($m^2$/g) | 0.3 | 5.1 |
| Space time W/F (g · min/ml) | $4 \times 10^{-3}$ | $6 \times 10^{-3}$ |
| Reaction temperature (°C) | 850 | 800 |
| Average $C_2$ formation rate ($\mu$mol/g · s) | 0.76 | 0.23 |
| Average total product formation rate ($\mu$mol/g · s) | 5.5 | 0.62 |
| Average $C_2$ selectivity | 24.8 | 53.3 |
| Average $C_2H_4/C_2$ percentage (%) | 0 | 9 |
| Average $O_2$ comsumption rate ($\mu$mol/g · s) | 9.72 | 1.04 |
| Percentage of $O_2$ comsumped (%) | 39 | 2 |

$C_2$ selectivity and percentage of ethylene in the $C_2$ products are plotted in Fig. 9 (the selectivity for carbon oxide is 100% minus the $C_2$ selectivity).

As shown in Fig. 8, the catalytic activity for both LSC and Li/MgO decreases with increasing methane run time. At 4 min, the catalytic activity for Li/MgO essentially diminishes. LSC is more active than Li/MgO for both partial and complete oxidation of methane. It remains catalytically active after 4 min of the methane run time. However, the $C_2$ selectivity of LSC is lower than that for Li/MgO. Furthermore, LSC produces no ethylene while about 10% of ethylene in $C_2$ products is observed in Li/MgO, as shown in Fig. 9. It should be noted that extremely high $C_2$ selectivity (about 90%) was found for LSC at 5 s of methane run time. Since the data at the very beginning may not be very accurate, the data at 5 s are not included in Figs. 8 and 9. The reaction kinetic data averaged over the four-minute period of the methane run time for LSC and Li/MgO are compared in Table 3.

The consumption rate of oxygen in the metal oxide during the methane run can be calculated from the formation rates of oxygen containing species (CO, $CO_2$ and $H_2O$) measured from the effluent stream. Figure 10 shows the results of the oxygen consumption rate corresponding to the data given in Figs. 8 and 9. The percentage of oxygen in the LSC consumed was calculated from the oxygen consumption rate data assuming that at time zero the weight of the sample corresponded to $La_{0.2}Sr_{0.8}CoO_{3-\delta}$ with zero nonstoichiometry (i.e., $\delta = 0$). For Li/MgO the percentage of oxygen consumed was calculated based on the total oxygen contained in Li/MgO (5% $Li_2O$–95% MgO). The results are also given in Fig. 10. The averaged oxygen consumption rate and total percentage of oxygen consumed for the 4-min methane run are summarized in Table 3.

A very small oxygen consumption rate is found for Li/MgO. In the whole process, less than 2% of oxygen in

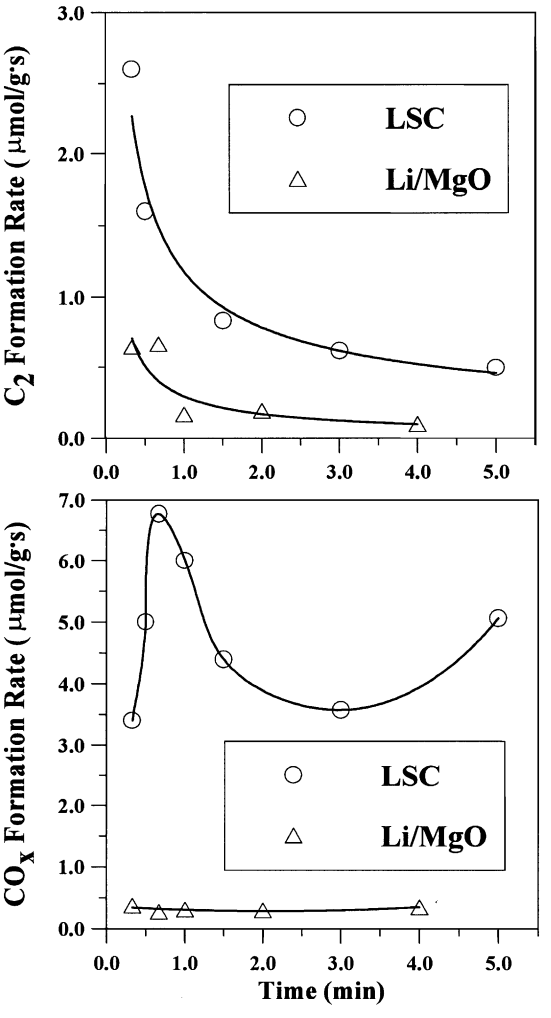


**FIG. 8.** Instant $C_2$ and $CO_x$ formation rate as a function of methane run time.

Li/MgO is consumed for oxidation reactions. As discussed earlier, it is generally agreed that $[Li^+O^-]$ is the active site for methane activation. $[Li^+O^-]$ sites are essentially present on the surface of the Li/MgO particles. At the beginning of the methane run, the surface of Li/MgO contains a large amount of the active sites. These sites are consumed very quickly by OCM when Li/MgO is exposed to methane. Since Li/MgO does not have the ability to retain and consequently release a considerable amount of active oxygen species in the cyclic mode, very limited oxygen is available in the bulk of Li/MgO particles to replace the consumed surface active sites. This results in a very sharp decrease of the $C_2$ formation rate on Li/MgO with the methane run time. With decreasing amount of the surface active sites, the $C_2$ selectivity also decreased. Nevertheless, the high initial $C_2$ formation rate and selectivity indicate that the surface of Li/MgO is very active and selective for OCM, consistent with the results observed on the cofeed experiments.

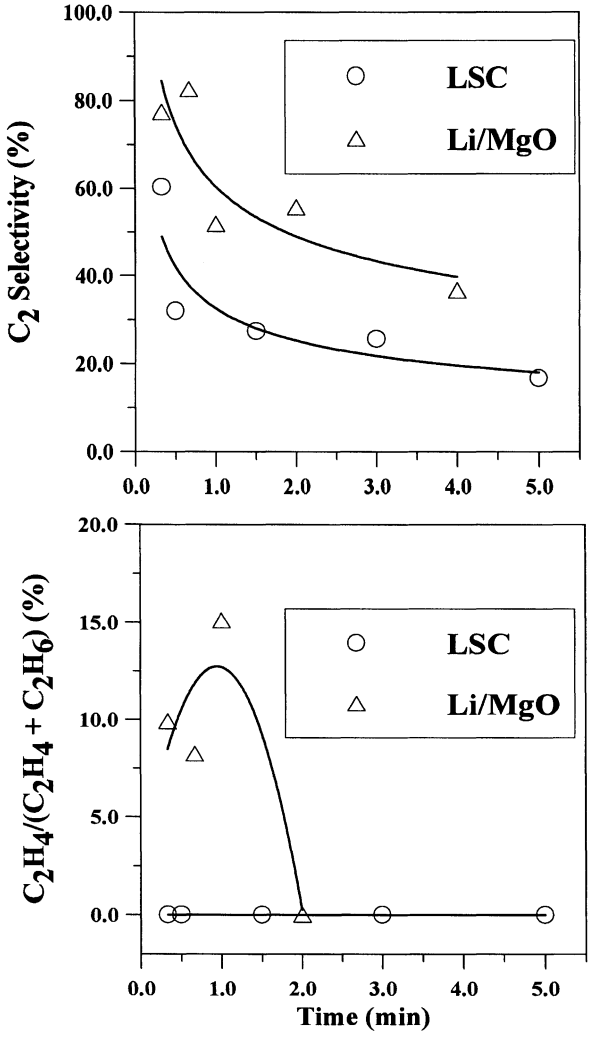


**FIG. 9.** $C_2$ selectivity and percentage of ethylene in $C_2$ as a function of methane run time.

Figure 11 shows transient TGA data for Li/MgO. The Li/MgO sample was exposed to the flow of oxygen in the time period from 0 to 400 min (curve A–B). In this period of time the weight of Li/MgO sample decreased continuously. This was apparently due to the loss of $Li_2O$ to the gas phase at 800°C since Li may sublime at temperatures lower than 1000°C. The average $Li_2O$ loss rate is estimated to be 0.007 gram of $Li_2O$ per gram of Li/MgO per hour. In the period from B to C shown in Fig. 11, the Li/MgO sample was exposed alternatively to methane flow and oxygen flow (each for a period of 5 min) with 2-min evacuation plus 2-min helium purge in between. There is essentially no variation of the sample weight in response to the alternation of the gas atmosphere. This confirms that Li/MgO does not have the ability to store and release oxygen.

Very different results on oxygen consumption are observed for LSC, as shown in Fig. 10. The oxygen consumption rate for LSC is much higher than that for Li/MgO. For

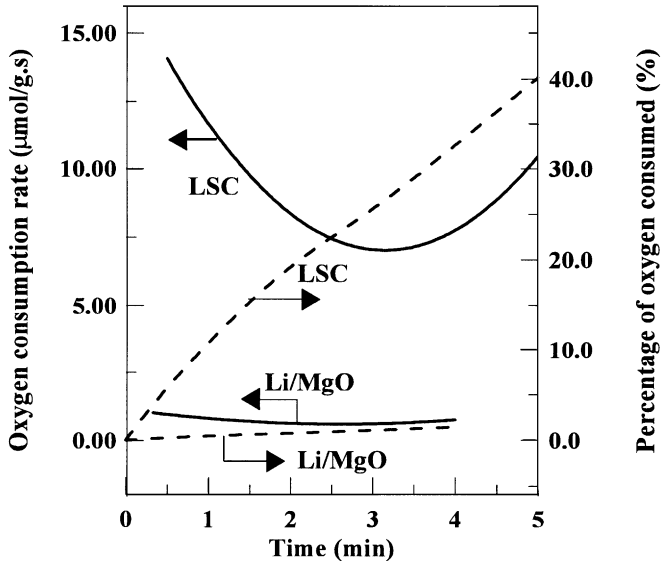


**FIG. 10.** Oxygen consumption rate and accumulated percentage of oxygen consumed as a function of methane run time.

the 5-min methane run, about 40% of oxygen in LSC is consumed by the reaction (see Table 3 and Fig. 10). The structure of LSC is very different from that of Li/MgO. The former is in the form of a solid solution containing a considerable amount of nonstoichiometric oxygen. The oxygen consumption rate for LSC ranges from 6 to 15 $\mu$mol/g · s.

Figure 12 shows transient TGA data for LSC exposed alternatively to the flow of oxygen (curve A–B, followed with a helium flow for 2 min), methane (curve B–C), and

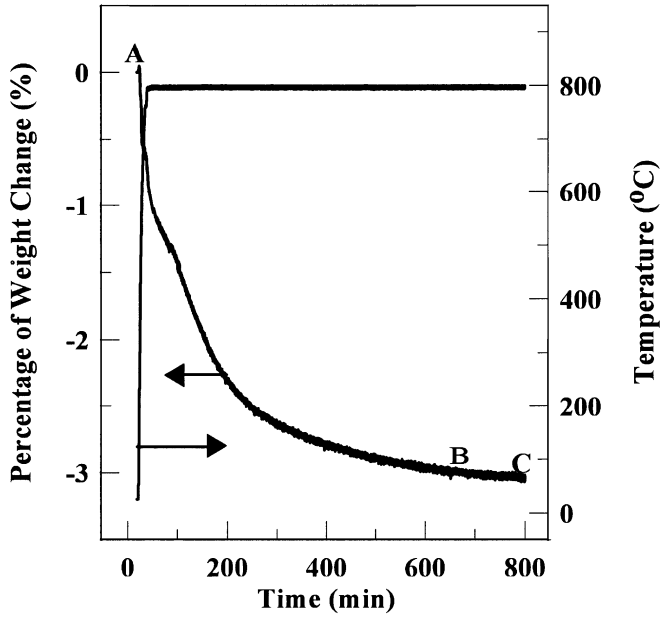


**FIG. 11.** Transient weight change and corresponding sample temperature for Li/MgO exposed to flow of oxygen (A–B) and methane (B–C).

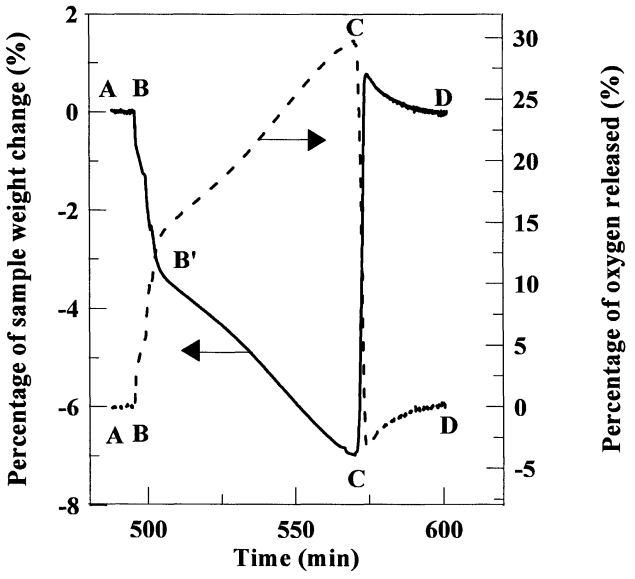


**FIG. 12.** Transient weight change and corresponding accumulated percentage of oxygen released from LSC sample exposed to the flow of oxygen (followed with helium for 2 min) (A–B), methane (B–C), and oxygen (C–D).

oxygen curve (C–D). The oxygen partial pressure in the flow of methane is not certain, but could be lower than $10^{-17}$ atm from the thermodynamic data calculated by Alcock *et al.* (19). The oxygen loss period (curve B–C) can be separated into a fast first oxygen loss period (B–B′) and a slow second oxygen loss period (B′–C). The oxygen absorption rate (C–D) is also very fast. It is interesting to note that curve C–D exhibits a peak at which the sample weight is about 0.5% higher than the initial weight of the sample. This is very likely due to the deposition of carbon on LSC when it is exposed to the flow of methane, which was also reported by other investigators (44). The weight becomes the same as the initial sample weight after about 25 min exposure to oxygen, indicating that the deposited carbon is oxidized and released to the gas phase. The appearance, color, and shape of the LSC particles after several cycles remained unchanged. These results confirm the large oxygen storage capacity of LSC and the reversibility of the oxygen desorption and absorption process even in the highly reducing environment. The equilibrium nonstoichiometry calculated from the TGA data shown in Fig. 12 are consistent with experimental findings reported in the literatures (45–47).

Comparing the oxygen consumption data for LSC exposed to pure methane, one finds that oxygen in LSC is consumed much faster in the packed-bed reactor (Fig. 10) than in the TGA reactor (Fig. 12). The times required for 10% and 30% of the oxygen consumed in the pack-bed reactor are respectively about 1 and 3 min, and in the TGA reactor about 5 and 60 min. Since under the experimental conditions diffusion of oxygen in the gas phase is much faster than that in the solid, the rate limiting step of the oxygen consumption process is the transport of oxygen from the bulk of the LSC particle to the gas adjacent the particle surface. Due to the difference in the reactor configuration, the interstitial velocity of the methane in the pack-bed reactor is about 12 cm/s, much larger than that in the TGA reactor (about 0.6 cm/s). During the methane run in the packed-bed reactor, the oxygen partial pressure in the gas phase adjacent to the particle surface is much lower than that when LSC is exposed to the methane stream in the TGA reactor. It is known that the oxygen transport rate in the mixed-conducting ceramic membrane is very sensitive to the oxygen partial pressure on the lower pressure side (22). Thus, the lower oxygen consumption rate in the TGA reactor is consistent with the characteristics of oxygen transport in mixed-conducting ceramics.

Table 4 compares the results for OCM on LSC and Li/MgO obtained in the cyclic feed mode and the cofeed mode. The space time in the cyclic feed operation is similar to that in the cofeed operation. For both materials, the cyclic feed operation gives a lower initial $C_2$ formation rate and a much higher initial $C_2$ selectivity than in the cofeed operation. It is reasonable to assume that at the very beginning of the cyclic feed operation the major reactions take place on the surface and essentially no carbon oxides are generated in the gas phase. The fact that the initial $C_2$ selectivity is smaller than 100% in the cyclic feed operation indicates considerable complete oxidation reactions occurring on the surface of the catalysts. The average $C_2$ formation rate of Li/MgO during the methane run in the cyclic feed operation is much smaller than that in the cofeed operation. This is due to the limited availability of the absorbed oxygen and lack of the mobile oxygen in the bulk phase to replace the consumed active sites. Because of very high initial $C_2$ selectivity of Li/MgO, the average $C_2$ selectivity during the

**TABLE 4**

**Comparison of the Results of OCM Operated in Cyclic Mode and Cofeed Mode**

| Material | $La_{0.2}Sr_{0.8}CoO_3$ | 5% Li/MgO |
|---|---|---|
| Reaction temperature (°C) | 850 | 800 |
| Cyclic mode | | |
| Space time W/F (g · min/ml) | $4 \times 10^{-3}$ | $6 \times 10^{-3}$ |
| Highest $C_2$ formation rate ($\mu$mol/g · s) | 2.60 | 0.67 |
| Average $C_2$ formation rate ($\mu$mol/g · s) | 0.76 | 0.23 |
| Highest $C_2$ selectivity (%) | 60.4 | 82.7 |
| Average $C_2$ selectivity (%) | 25.6 | 53.3 |
| Average $C_2H_4/C_2$ ratio | ≈0 | 0.1 |
| Average $CO/CO_x$ ratio | ≈0 | ≈0 |
| Cofeed mode ($CH_4/O_2 = 2.9$) | | |
| Space time W/F (g · min/ml) | $4 \times 10^{-3}$ | $3.7 \times 10^{-2}$ |
| $C_2$ formation rate ($\mu$mol/g · s) | 6.00 | 1.1 |
| $C_2$ selectivity (%) | 54.0 | 51.4 |
| $C_2H_4/C_2$ ratio | 0.64 | 0.78 |
| $CO/CO_x$ ratio | 0.04 | ≈0 |

entire period of methane run in the cyclic feed operation is still slightly larger than that in the cofeed one. The Li/MgO sample in the cyclic feed operation gives much less ethylene and CO than in the cofeed one. It is expected that Li/MgO will lose its activity and selectivity for OCM after more than 5 min of the methane run in the cyclic feed operation.

In the cyclic feed mode the instant $C_2$ formation rate for LSC decreases sharply in the initial period of methane run time. The decrease of the $C_2$ formation rate is substantially slowed at the longer methane run time. The transport of oxygen from the bulk of the LSC particles to the particle surface could be the rate-limiting step after the initial period of the methane run time. The appreciable average $C_2$ and carbon oxide formation rates for LSC in the cyclic feed mode indicate that the surface of LSC is still rather active for methane oxidation reactions. However, the average $C_2$ selectivity, $C_2H_4/C_2$ ratio, and $CO/CO_x$ ratio for LSC in the cyclic feed mode are much lower than in the cofeed mode. These suggest that in the cyclic feed mode LSC maintains appreciable activity but loses the selectivity for partial oxidation of methane as compared to the cofeed mode.

As discussed early it is known that mixed-conducting ceramics exhibiting *p*-type electronic conductivity are selective for OCM (38). The electronic conduction mechanism for the mixed-conducting ceramics, including LSC, changes from *p*-type to *n*-type with decreasing oxygen partial pressure (48). The oxygen partial pressure at which the transition of electronic conduction mechanism occurs can be estimated from the electronic conductivity versus oxygen partial pressure data. The transition $P_{O_2}$ for a similar material, $La_{0.6}Sr_{0.4}Co_{0.2}Fe_{0.8}O_3$, estimated from the conductivity data measured recently by Anderson's group (39), decreases from $10^{-9}$ to $10^{-13}$ atm as temperature changes from 1200 to 1000°C. Considering the temperature effect and slight difference in composition, the transition $P_{O_2}$ for LSC at 850°C could be around $10^{-16}$ atm, below which LSC is an *n*-type electronic conductor. In the cofeed mode, the oxygen partial pressure is relatively high because of the presence of oxygen in the feed gas. LSC in the cofeed mode is a *p*-type electronic conductor. However, in the cyclic mode the LSC sample is exposed to pure methane with a much lower oxygen partial pressure, and may become an *n*-type electronic conductor and nonselective for OCM (38).

It should be pointed out that during the methane run in the cyclic feed operation the exact oxygen partial pressure in the gas phase, though known to be lower than that in the cofeed operation, is not certain. The oxygen partial pressure in this case is in fact determined by kinetic factors, rather than by equilibrium relations. In the membrane reactor for OCM, the oxygen partial pressure in the gas phase adjacent the surface of membrane exposed to methane could be very low, determined primarily by the ratio of the oxygen permeance to the reaction rate (21). The surface of LSC may no longer possess good catalytic selectivity for OCM in the membrane reactor with lower oxygen partial pressure in the reacting gas. Work continues in this laboratory using the approach described here to search for membrane materials with desired OCM catalytic properties and oxygen pereability, and the results on other materials will be reported in subsequent publications.

## CONCLUSIONS

In the steady state cofeed operation and at 800–850°C and methane to oxygen ratio of 2.9, the $C_2$ selectivity, yield, and space time yield for $La_{0.8}Sr_{0.2}CoO_3$ (LSC) are in the range of 40–56%, 12–14% and 6–7 $\mu$mol/g.s, respectively. The $C_2$ space time yield for LSC is larger than that for Li/MgO, and the $C_2$ selectivity and yield for the former are similar to those for the latter. $SrCo_{0.8}Fe_{0.2}O_3$ (SCF) exhibits much poorer catalytic properties for OCM in the experimental conditions studied as compared to LSC.

The instant $C_2$ selectivity and activity for OCM on LSC and 5% Li/MgO as a function of methane run time were measured respectively at 850°C and 800°C after the materials saturated with oxygen were exposed to pure methane. For both materials the unsteady-state operation gives a smaller initial OCM activity and a much larger initial $C_2$ selectivity as compared with the cofeed steady state operation. The initial $C_2$ selectivity data in the unsteady state operation also suggest considerable complete oxidation reactions occurring on the surface of these two materials.

When exposed to pure methane, Li/MgO quickly loses OCM activity and selectivity in the unsteady state operation due to rapid consumption of active sites. The surface of LSC maintains appreciable OCM activity when it is exposed to pure methane, but exhibits much poorer $C_2$ selectivity as compared to the steady state cofeed operation. The OCM catalytic properties of these two materials observed on the unsteady state packed-bed reactor are consistent with transient TGA data showing oxygen storage capacity and reversibility of absorption and desorption of oxygen of these materials at high temperatures.

OCM catalytic properties of the perovskite-type mixed-conducting ceramic membrane materials appeared to be determined by the synthesis method, surface oxygen exchange rate, and electronic conduction mechanism. Since the electronic conduction mechanism of the perovskite-type ceramics are strongly dependent of the oxygen partial pressure in the reaction atmosphere, their OCM catalytic properties are sensitive to the reaction conditions and reactor mode which affect the oxygen partial pressure in the atmosphere in contact with the surface of the catalyst.

Among the three catalysts studied, LSC and Li/MgO, but not SCF, are good catalysts for use in the conventional cofeed packed-bed reactor in terms of their catalytic properties. The OCM catalytic properties of LSC deteriorate in the reducing atmosphere. The surface of the LSC

membrane may become nonselective for OCM in the membrane reactor if the LSC membrane used does not have sufficiently high oxygen permeance.

## ACKNOWLEDGMENTS

This project was supported by Amoco Corporation and National Science Foundation (CAREER award). The perovskite type ceramic samples studied in this work were kindly provided by Dr. Henny Bouwmeester of University of Twente.

## REFERENCES

1. Amenomiya, Y., Birss, V. I., Goledzinowski, M., Galuszka, J., and Sanger, A. R., *Catal. Rev. Sci. Eng.* **32**, 163 (1990).
2. Ray, A., Tonkovich, A. L., Aris, R., and Carr, R. W., *Chem. Eng. Sci.* **45**, 2431 (1990).
3. Tonkovich, A. L., Carr, R. W., and Aris, R., *Science* **262**, 221 (1993).
4. Jiang, Y., Yentekakis, I. V., and Vayenas, C. G., *Science* **264**, 1563 (1994).
5. Hazbun, E. A., U.S. Patent 4,791,079, 1988.
6. Hazbun, E. A., U.S. Patent 4,827,071, 1989.
7. Mieville, R. L., U.S. Patent 5,276,237, 1994.
8. Nozaki, T., Hashimoto, S., Omata, K., and Fujimoto, K., *Ind. Eng. Chem. Res.* **32** (1993).
9. Nozaki, T., and Fujimoto, K., *AIChE J.* **40**, 870 (1994).
10. Nozaki, T., Yamazaki, O., Omata, K., and Fujimoto, K., *Chem. Eng. Sci.* **47**, 2945 (1992).
11. Lafarga, D., Santamaria, J., and Menendez, M., *Chem. Eng. Sci.* **49**, 2005 (1994).
12. Coronas, J., Menendez, M., and Santamaria, J., *Chem. Eng. Sci.* **49**, 2015 (1994).
13. Saracco, G., and Specchia, V., *Catal. Rev. Sci. Eng.* **36**, 305 (1994).
14. ten Helshof, J. E., Bouwmeester, H. J. M., and Verweeij, H., *Appl. Catal. A* **130**, 195 (1995).
15. Nagamoto, H., Hayashi, K., and Inoue, H., *J. Catal.* **126**, 671 (1990).
16. Kuchynka, D. J., Cook, R. L., and Sammells, A. F., *J. Electrochem. Soc.* **138**, 1284 (1991).
17. Eng, D., and Stoukides, M., *J. Catal.* **130**, 306 (1991).
18. Tonkovich, A. L., Secker, R. B., Reed, E. L., Roberts, G. L., and Cox, J. L., *Sep. Sci. Technol.* **30**, 1609 (1995).
19. Balachandran, U., Dusek, J. T., Mieville, R. L., Poeppel R. B., Kleefisch, M. S., Pei, S., Kobylinski, T. P., Udovich, C. A., and Bose, A. C., *Appl. Catal. A* **133**, 19 (1995).
20. Pei, S., Kleefisch, M. S., Kobylinski, T. P., Faber, J., Udovich, C. A., Zhang-McCoy, V., Dabrowski, B., Balachandran, U., Mieville, R. L., and Poeppel, R. B., *Catal. Lett.* **30**, 201 (1995).
21. Wang, W., and Lin, Y. S., *J. Membrane Sci.* **103**, 219 (1995).
22. Lin, Y. S., Wang, W., and Han, J., *AIChE J.* **40**, 786 (1994).
23. Burggraaf, A. J., Bouwmeester, H. J. M., Boukamp, B. A., Uhlhorn, R. J. R., and Zaspalis, V. T., *in* "Science of Ceramic Interfaces" (J. Norwony, Ed.), pp. 525–568, North-Holland, Amsterdam, 1991.
24. Teraoka, Y., Zhang, H., Furukawa, S., and Yamazoe, N., *Chem. Lett.*, 1743 (1985).
25. Kruidhof, H., Bouwmeester, H. J. M., Doorn, R. H. E. v., and Burggraaf, A. J., *Solid State Ionics* **63/65**, 816 (1993).
26. Bouwmeester, H. J. M., Kruidhof, H., and Burggraaf, A. J., *in* "Solid State Ionics, 9th Proceeding (SSI)," September 1993.
27. Itoh, N., Kato, T., Uchida, K., and Haraya, K., *J. Membrane Sci.* **92**, 239 (1994).
28. Hayakawa, T., Orita, H., Shimizu, M., Takehira, K., Andersen, A. G., Nomura, K., and Ujihira, Y., *Catal. Lett.* **16**, 359 (1992).
29. Alcock, C. B., Carberry, J. J., Doshi, R., and Gunasekaran, N., *J. Catal.* **143**, 533 (1993).
30. Omata, K., Yamazaki, O., Tomita, K., and Fujimoto, K., *J. Chem. Soc. Chem. Commun.*, 1647 (1994).
31. Blank, D. H. A., Kruidhof, H., and Flokstra, J., *Phys. D. Appl. Phys.* **21**, 226 (1988).
32. Ito, T., Wang, J. X., Lin, C. H., and Lunsford, J. H., *J. Am. Chem. Soc.* **107**, 5062 (1985).
33. Korf, S. J., Roos, J. A., Bruijn, N. A., Ommen, J. G., and Ross, J. R. H., *Catal. Today* **2**, 535 (1988).
34. Lee, J. S., and Oyama, S. T., *Catal. Rev. Sci. Eng.* **30**, 249 (1988).
35. Hutchings, G. J., Scurrell, M. S., and Woodhouse, J. R., *Chem. Soc. Rev.* **18**, 251 (1989).
36. Fox, J. M., *Catal. Rev. Sci. Eng.* **35**, 169 (1993).
37. McCarty, J. G., and Wise, H., *Catal. Today* **8**, 231 (1990).
38. Zhang, Z., Verykios, X. E., and Baerns, M., *Catal. Rev. Sci. Eng.* **36**, 507 (1994).
39. Tai, L. W. F., "Oxides of $La_{1-x}Co_xCo_{1-y}Fe_yO_3$ for Oxygen and Electrical Delivery Systems," Ph.D. Thesis, University of Missoui-Rolla, Rolla, Missouri (1994).
40. Voskresneskaya, E. N., Roguleva, V. G., and Anshits, A. G., *Catal. Rev. Sci. Eng.* **37**, 101 (1995).
41. Keller, G. E., and Bhasin, M. M., *J. Catal.* **73**, 9 (1982).
42. Gaffney, A. M., Jones, C. A., Leonard, J. J., and Sofranko, J. A., *J. Catal.* **114**, 422 (1988).
43. Miro, E. E., Kalenik, Z., Santamaria, J., and Wolf, E. E., *Catal. Today* **6**, 511 (1990).
44. Yamashita, H., Machida, Y., and Tomita, A., *Appl. Catal. A. Gen.* **79**, 203 (1991).
45. Mizusaki, J., Mima, Y., Yamauchi, S., Fueki, K., and Tayawa, H., *J. Solid State Chem.* **80**, 102 (1989).
46. Van Hassel, B. A., Kawada, T., Sakia, N., Yookawa, H., Dokiya, M., and Bouwmeester, H. J. M., *Solid State Ionics* **66**, 295 (1993).
47. Yamazoe, N., Teraoka, Y., and Seiyama, T., *Chem. Lett.*, 1767 (1981).
48. Gellings, P. J., and Bouwmeester, H. J. M., *Catal. Today* **12**, 1 (1992).